Research Article

Chemical Review and Letters
journal homepage: www.chemrevlett.com
ISSN (online): 2645-4947 (print) 2676-7279

Investigation of hot corrosion behavior of NiCoCrAlY coatings in molten Na_2SO_4 - V_2O_5 at 900°C

Vahid Razmgir[1, *]

[1]*Department of Materials Engineering, Faculty of Mechanical Engineering, University of Tabriz, Tabriz, Iran.*

ARTICLE INFO

Article history:
Received 09 June 2025
Received in revised form 04 August 2025
Accepted 13 August 2025
Available online 15 August 2025

Keywords:
NiCrAlY
Metal interface coating
Nickel based superalloy (Inconel718LC)
Electrochemical deposition
Hot corrosion

ABSTRACT

This study investigates the hot corrosion resistance of NiCoCrAlY coatings deposited on Inconel 718LC superalloy in a molten Na_2SO_4-50%V_2O_5 environment at 900 °C. The coatings were fabricated via electrodeposition using varying current densities (20 and 30 mA/cm^2) and NiCrAlY powder concentrations (10, 20, and 30 g/l). Results revealed that coatings with 20 g/l powder concentration and a current density of 20 mA/cm² exhibited optimal performance, demonstrating superior corrosion resistance due to the formation of protective Al_2O_3 and Cr_2O_3 scales, as well as spinel phases such as $NiCr_2O_4$. In contrast, samples with lower powder concentrations (10 g/l) suffered complete degradation owing to insufficient aluminum content. The corrosion mechanism involved the decomposition of molten salts into aggressive compounds (e.g., $NaVO_3$ and $NaAlO_2$), which deteriorated the protective layers. Additionally, the formation of metallic sulfides (e.g., NiS and CrS) and acid-base reactions accelerated corrosion. SEM and XRD analyses confirmed that the optimized coatings possessed a uniform microstructure and stable protective phases. This research highlights that controlling deposition parameters and coating composition can significantly enhance the service life of Superalloys in high-temperature corrosive environments.

1. Introduction

Nickel-based Super alloys are widely used in gas turbine and aircraft engine components owing to their exceptional mechanical properties and high corrosion resistance [1, 2]. However, a significant challenge emerges when these components are exposed to corrosive gases from sulfur-rich fuels or molten salts in high-temperature heat transfer systems, leading to gradual degradation of their favorable properties [3]. Under such conditions, corrosive compounds such as NaCl, KCl, V_2O_5, and Na_2SO_4 form surface deposits on the alloy, promoting a phenomenon known as hot corrosion, where destructive chemical reactions occur at the alloy-salt interface [4]. Moreover, while certain alloying elements enhance mechanical performance, they often compromise corrosion resistance [5, 6].

Serious issues arise when complex mixtures of molten sodium sulfate (Na_2SO_4) and vanadium pentoxide (V_2O_5) enter power generation systems due to low-quality fuel. Na_2SO_4 can be transported with air to the turbine inlet or may form through reactions between sodium chloride (NaCl) and sulfur impurities in the fuel [7]. During combustion, vanadium porphyrins present in the fuel convert to V_2O_5. The reaction between Na_2SO_4 and V_2O_5 produces new compounds with eutectic temperatures below 600°C [8]. These eutectic compounds readily melt and deposit on turbine blades, causing severe corrosion with significant consequences [9].

MCrAlY (M = Ni, Co) coatings have recently attracted significant research attention due to their remarkable effectiveness in combating corrosion phenomena. These coatings serve dual functions: they act as bond coats in thermal barrier coating (TBC) systems while also being employed as standalone coatings to prevent oxidation and corrosion in high-temperature environments [10]. The protective mechanism of these coatings in corrosive environments is particularly noteworthy. Chromium and aluminum elements in the coating composition spontaneously form a continuous, protective layer of corrosion products that acts as an effective barrier against corrosion propagation [11]. Another crucial aspect is the role of yttrium (Y) which, even in trace amounts, accelerates the formation of the

* Corresponding author E-mail: v.razmgir_1991@tabrizu.ac.ir
https://doi.org/10.22034/crl.2025.529300.1629

protective layer through Y_2O_3 formation while simultaneously enhancing the adhesion between this layer and the substrate [12].

Among the constituent elements of these coatings, cobalt holds a unique position. While conventional wisdom suggests that cobalt enhances the formation of protective oxides such as Cr_2O_3 and Al_2O_3, recent studies including the work by Sundaresan et al [13]. Have demonstrated that excessive cobalt oxides in the corrosion layer may have adverse effects, potentially compromising the corrosion resistance of NiCoCrAlY coatings [14]. These findings highlight the need to re-examine the precise role of cobalt oxides. Despite significant progress in this field, numerous aspects remain unexplored. To date, most research has focused on the corrosion behavior of coatings under thin salt films at elevated temperatures, while the corrosion mechanisms induced by molten salts in MCrAlY coatings remain poorly understood and warrant further in-depth investigation [15].

The systematic study of corrosion mechanisms and the development of effective inhibitors are critical for enhancing the durability and service life of structural materials in aggressive environments [16-18]. The hot corrosion resistance of coatings primarily depends on the formation of a surface corrosion layer that acts as an ionic barrier, separating the coating from the corrosive environment [19]. This dependence underscores the critical importance of thoroughly investigating the characteristics of this protective layer to fully understand hot corrosion mechanisms. Currently, conventional evaluation methods for corrosion layers in MCrAlY coatings are predominantly ex situ and conducted at ambient temperatures - an approach that presents significant limitations in accurately assessing the protective capabilities of these layers. Crucially, hot corrosion is inherently a complex electrochemical process involving electron transfer mechanisms and lattice defect migration. Despite these advances, it should be noted that research investigating the hot corrosion properties of MCrAlY coatings exposed to molten salts remains remarkably limited and insufficient to date [20].

This study investigates the development and fabrication of NiCoCrAlY coatings on Inconel 718LC superalloy substrates. This advanced superalloy is specialized for gas turbine components and aircraft engine turbine disks, exhibiting exceptional mechanical properties due to γ' (Al_3Ni) intermetallic precipitates that strengthen the γ (Ni, Co) matrix [21]. While its standard operational temperature range is typically up to 850°C, it can withstand emergency conditions for limited durations at temperatures as high as 900 °C [22].

For coating deposition, electrochemical deposition was selected as the optimal technique, offering advantages such as uniform and controlled thickness, enhanced corrosion and oxidation resistance, improved surface properties, and relatively low production costs-making it ideal for high-temperature-resistant coatings [23]. During experimental testing, the coatings' hot corrosion behavior was rigorously evaluated under extreme conditions (900°C) in a highly corrosive molten salt environment of Na_2SO_4-50%V_2O_5 [24].

The 900°C test temperature was chosen to align with the operational conditions of Inconel 718LC superalloy in gas turbines and jet engines, where the critical emergency threshold typically ranges between 850-900°C [25]. This temperature simulates severe yet realistic conditions, maximizing the likelihood of corrosive molten salt formation (e.g., Na_2SO_4- V_2O_5). Additionally, it enables a comprehensive study of acid/base fluxing mechanisms, which may remain incomplete at lower temperatures. This selection is further supported by prior research, as 900°C strikes an optimal balance between rapid coating degradation and real-world operational conditions [26].

2. Materials and Methods

2.1. Preparation of Samples

The nickel-based superalloy Inconel 718LC (chemical composition provided in Table 1) served as the substrate for coating deposition. Specimens were precision-cut into rectangular cuboids with dimensions of 15 mm (length) × 10 mm (width) × 3 mm (thickness) and subsequently underwent rigorous surface preparation. This multi-step process included: (1) abrasive grinding with progressively finer grits to eliminate surface oxides and topographical irregularities, (2) ultrasonic degreasing in acetone and ethanol to remove organic contaminants, (3) thorough rinsing with deionized water, (4) chemical etching in a 10% HCl solution for surface activation, and (5) final ultrasonic cleaning in deionized water to ensure complete removal of processing residues.

Table 1. Percentage of elements and chemical composition of nickel base superalloy

Ni	**Cr**	**Fe**	**Nb**	**Mn**	**Mo**	**S**	**Si**
Balance	18.9	17.79	4.35	0.0372	3.02	0.0011>	0.108
V	**W**	**Ta**	**Mg**	**Zr**	**Sb**	**Zn**	**Sn**
0.0525	0.0141	0.0386	0.0088	0.0097	0.0015>	0.0071	0.0005>
C	**Co**	**Al**	**Ti**	**Cu**	**B**	**P**	**As**
0.0253	0.0674	0.45	0.969	0.048	0.0051	0.0129	0.002

2.2. Deposition conditions

Composite Ni-Co/NiCrAlY alloy coatings were electrodeposited using a Watts bath containing dispersed NiCrAlY particles at controlled concentrations. To optimize the coating properties, two key parameters were systematically varied: (1) the concentration of NiCrAlY powder in the Watts bath (10, 20, and 30 g/l) and (2) the applied current density (20, 30 mA/cm^2), as detailed in Table 1. The first letter (A, B, C) indicates the applied current density level in mA per square centimeter: A: Current density of 10 mA/cm^2, **B:** Current density of 20 mA/cm^2 and **C:** Current density of 30 mA/cm^2. The subsequent number (10, 20, 30) represents the concentration of NiCrAlY powder in the electrolyte solution in grams per liter. All other deposition conditions were maintained constant based on established literature values: bath temperature at 45 °C, pH at 3.5, stirring speed at 160 rpm, and deposition duration fixed at 2 hours to ensure consistent coating formation across all experimental runs.

To ensure complete dissolution of NiCrAlY particles within the coating matrix and achieve uniform chemical composition, the coated specimens underwent homogenization treatment in an argon atmosphere using a tube furnace (Model TF5/40-1250) at 1100°C for 2 hours. Prior to heat treatment, all samples were thoroughly cleaned with ethanol to remove surface contaminants. The furnace pressure was maintained at 2.5 bar during the entire process, with titanium plates strategically positioned between specimens to prevent oxidation. Following the homogenization treatment at 1100°C, the specimens were furnace-cooled to room temperature to avoid thermal shock and preserve the microstructural integrity.

2.3. Hot Corrosion Resistance

The hot corrosion resistance of the fabricated coatings was evaluated using a corrosive salt mixture composed of Na_2SO_4-50%V_2O_5 (composition details provided in Table 2 and 3). Approximately 20 mg/cm^2 of the salt mixture was uniformly applied to the specimen surfaces using a circular stencil. The salt-coated specimens were then placed in a muffle furnace, which was heated to 900°C and maintained at this temperature for 4 hours (see Figure 1). Following the isothermal exposure, the furnace was turned off, and the specimens were slowly cooled inside the furnace to prevent thermal shock. After reaching ambient temperature, the specimens were immersed in boiling water for 30 minutes to remove residual salts, facilitating subsequent microscopic examination, structural analysis, and characterization of hot corrosion products.

2.4. Characterization

The coating morphology and structure following homogenization treatment and hot corrosion testing were examined using a CAMSCAN MV2300 scanning electron microscope (SEM) (Czech Republic) equipped with an Oxford energy-dispersive X-ray spectroscopy (EDS) system (UK) for compositional analysis.

Table 2. Electrochemical deposition conditions

Current Density	**B (20 mA/cm^2)**			**C (30 mA/cm^2)**		
Concentration of NiCrAlY Powder in the Bath (g/l)	10	20	30	10	20	30
Symbol	B_{10}	B_{20}	B_{30}	C_{10}	C_{20}	C_{30}

Table 3. Characteristics of salts used for hot corrosion testing

Salt type	**Melting point (C°)**	**Density (g/cm^3)**	**Purity (%)**	**Manufacturer**
Na_2SO_4	888	2.70	99% <	Merck
V_2O_5	690	3.35	98% <	Sigma

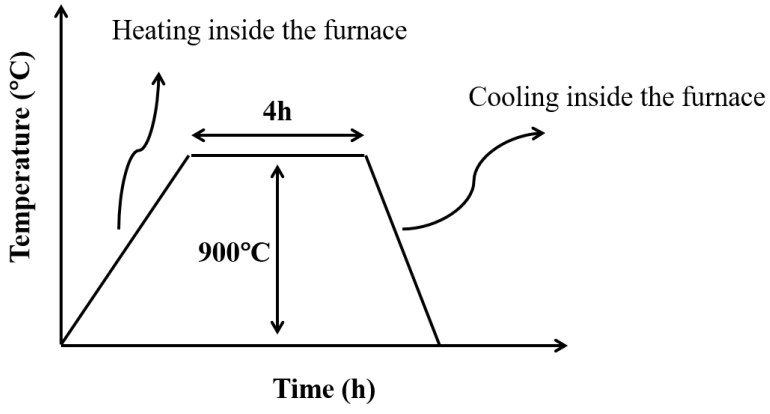

Fig. 1. Hot corrosion cycle program.

Three distinct analytical techniques were employed: (1) elemental mapping to investigate the spatial distribution of elements within the coating matrix and assess salt-induced degradation patterns, (2) line-scan analysis to evaluate elemental distribution across coating cross-sections, and (3) point analysis for localized compositional measurements. Phase identification was performed using a Bruker D8 Advance X-ray diffractometer (XRD) to characterize the crystalline phases formed during both homogenization and hot corrosion processes.

3. Results and Discussion

Figure 2(a) illustrates the uniform deposition of a 20 mg/cm^2 Na_2SO_4-50%V_2O_5 corrosive salt mixture on homogenized coating surfaces using a circular stencil for hot corrosion evaluation. Figure 2(b) displays the surface morphology of the coated superalloy (prepared at 20 mA/cm^2 current density and 20 g/l powder concentration) after a 2-hour homogenization treatment. Notably, the coating retained its characteristic silver hue and surface roughness following argon-atmosphere homogenization, indicating effective oxidation protection during thermal processing. Figure 2(c) presents the post-hot-corrosion appearance (900°C exposure) of specimens prepared under identical parameters. While salt exposure induced surface darkening and loss of metallic luster, no microcracks or fractures were observed in salt-contacted regions after cleaning, confirming the coating's structural integrity under aggressive conditions.

Figure 3 presents macroscopic images of NiCoCrAlY coatings prepared at various current densities and powder concentrations following 4-hour hot corrosion testing at 900°C. The coatings' appearance transitioned from their original silver color to black after exposure. Notably, coatings deposited at 10 g/l NiCrAlY powder concentration exhibited complete degradation, attributable to insufficient aluminum content (~ 4.5 wt%) in the cross-section. This aluminum deficiency prevents the formation of a protective alumina scale, resulting in poor hot corrosion resistance. In contrast, other specimens maintained coating integrity without substrate delamination, demonstrating effective protection under identical test conditions.

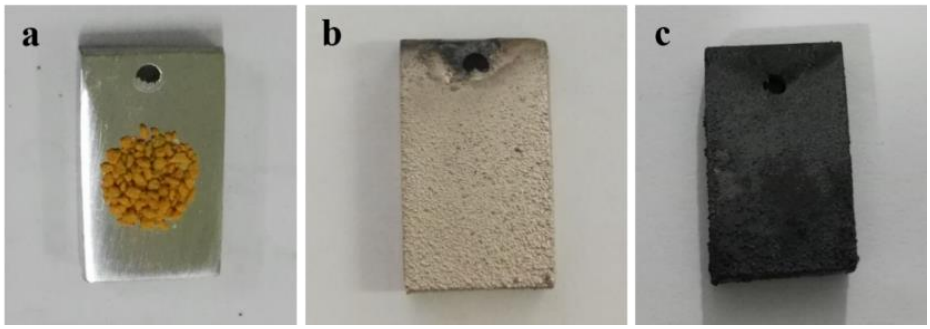

Fig. 2. (a). Placement of the corrosive salt mixture, (b). Appearance of the coated superalloy after 2 hours of homogenization, (c). Appearance of the coating after hot corrosion treatment at 900°C.

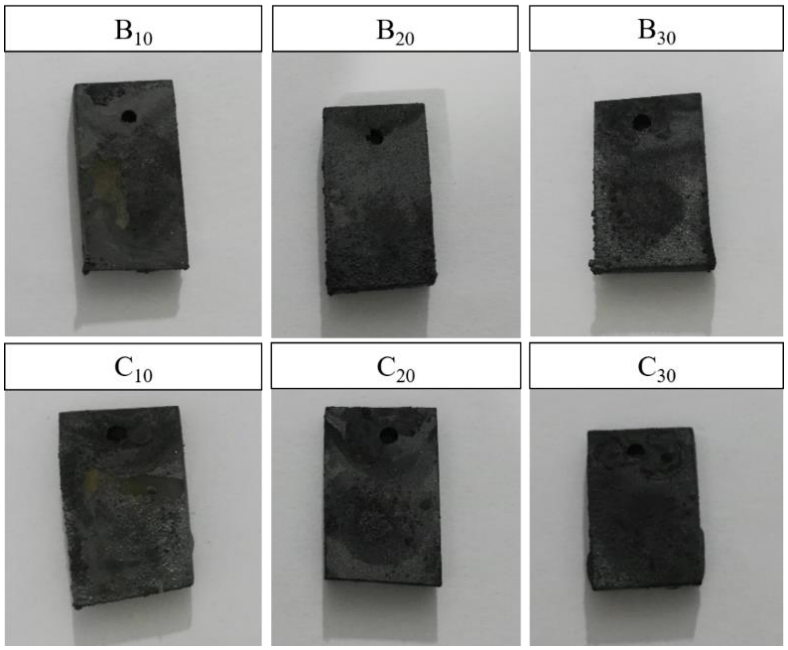

Fig. 3. Appearance of samples after hot corrosion test**.**

Figure 4 presents scanning electron micrographs of the coated specimen (prepared at 20 mA/cm^2 current density and 20 g/l powder concentration) following homogenization (2 h) and subsequent hot corrosion testing (4 h at 900°C), comparing pre- and post-washing conditions. Previous studies on NiCrAlY and MCrAlY coatings have demonstrated that optimal powder concentrations typically range between 10 to 40 grams per liter, though this value depends on the specific conditions and system employed. In corrosive environments such as molten salts (Na_2SO_4-50%V_2O_5), moderate concentrations of approximately 20 grams per liter exhibit superior performance by enabling uniform distribution and preventing particle aggregation.

The unwashed surface morphology (Figure. 4a) reveals flake-like structures of the Na_2SO_4-50%V_2O_5 salt mixture, critically without inducing microcracks, fractures, or delamination in the coating structure. This structural integrity was maintained after salt removal (Figure. 4b), with no observable microcracks on the cleaned surface. Energy-dispersive X-ray spectroscopy (EDS) mapping (Figure. 4c) further confirms the presence of salt-derived elements (Na, V, S) on the corroded surface, verifying their interaction during hot corrosion exposure. Superalloys typically undergo two distinct stages of hot corrosion:

(1) Initiation

(2) Propagation

All corrosion-resistant alloys degrade through these sequential stages, necessitating the implementation of selective oxidation strategies to enhance oxidation and corrosion resistance.

During hot corrosion testing above 890°C, the Na_2SO_4-50%V_2O_5 salt mixture melts due to the relatively low melting points of its constituents (Na_2SO_4: 888°C; V_2O_5: 690°C), forming both acidic and basic fluxing agents on the specimen surface. The hot corrosion mechanism in the presence of this salt mixture involves high-temperature decomposition of molten Na_2SO_4, generating sulfur oxides (SO_2/SO_3) and sodium oxide (Na_2O) flux.

$$Na_2SO_4\,(l) \rightarrow Na_2O\,(l) + SO_3\,(g) \quad (1)$$

$$2SO_3\,(g) \rightarrow 2SO_2\,(g) + O_2\,(g) \quad (2)$$

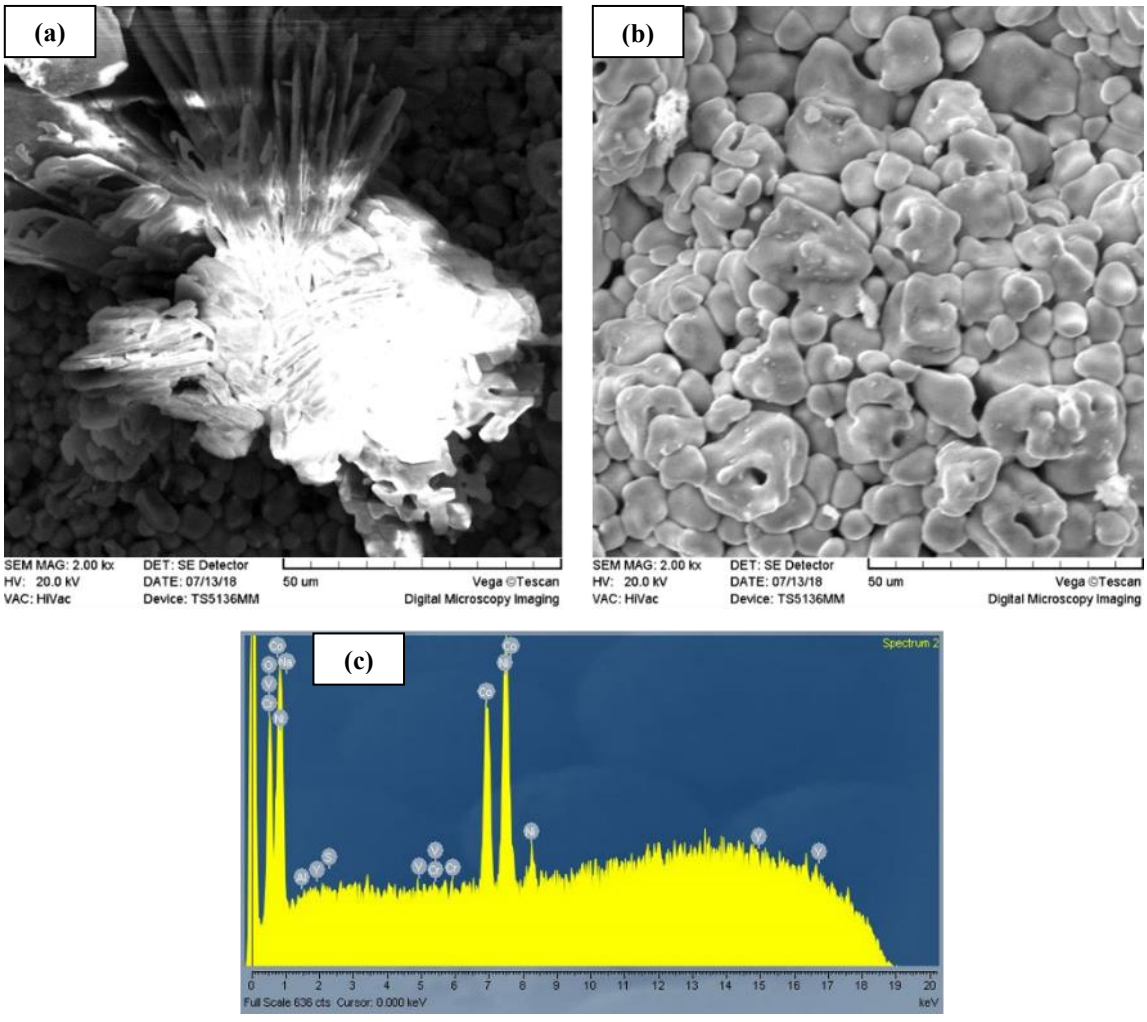

Fig. 4. (a) and (b) show SEM images of samples before and after washing, and (c) shows the spectroscopic image of the energy distribution of the surface under hot corrosion.

Sulfate and sulfite ions (SO_4^{2-}/SO_3^{2-}) can penetrate the alloy matrix, forming brittle metal sulfides (e.g., NiS, CrS, CoS). These sulfide phases significantly compromise oxide scale adhesion through two primary mechanisms: (1) creating weak interfacial boundaries at the oxide-alloy interface, and (2) generating volume mismatches due to their distinct crystallographic structures. The resulting loss of protective oxide cohesion accelerates spallation and exposes fresh metal surfaces to continued corrosive attack.

$$3Ni\ (s) + SO_2\ (g) \rightarrow NiS\ (l) + 2NiO\ (l) \quad (3)$$

$$5Co\ (s) + 2SO_2\ (g) \rightarrow 2CoS\ (l) + Co_3O_4\ (l) \quad (4)$$

$$7Cr\ (s) + 3SO_2\ (g) \rightarrow 3CrS\ (l) + 2Cr_2O_3\ (l) \quad (5)$$

The newly formed sodium oxide (Na_2O) rapidly reacts with V_2O_5, producing low-melting-point compounds (e.g., sodium metavanadate, $NaVO_3$, melting point ~ 630°C) that readily spread across the metal surface. More critically, Na_2O reacts with the protective alumina (Al_2O_3) scale in the coating system to form corrosive sodium aluminate ($NaAlO_2$), which: (1) disrupts the continuity of the protective oxide layer, and (2) creates ionic pathways for accelerated corrosive attack. This dual reaction mechanism significantly compromises the coating's long-term durability in high-temperature service environments.

$$Na_2O\ (l) + V_2O_5\ (l) \rightarrow 2NaVO_3\ (l) \quad (6)$$

$$Na_2O\ (l) + Al_2O_3\ (l) \rightarrow 2NaAlO_2\ (l) \quad (7)$$

The acidic oxide V_2O_5 reacts with protective oxides (Cr_2O_3, Al_2O_3, and NiO) in Inconel 718LC to form molten vanadates that initiate a three-stage degradation process: first, these vanadate compounds dissolve the protective oxide scale through acidic fluxing; second, they selectively deplete chromium concentration in the oxide layer; and third, they accelerate corrosion rates by continuously exposing fresh metal surfaces to the corrosive environment. This self-propagating mechanism becomes particularly severe in high-temperature operating conditions (typically above 700°C) where the molten vanadates maintain sufficient fluidity to penetrate deeper into the alloy substrate, ultimately leading to catastrophic failure of turbine components through rapid section loss and microstructural degradation.

$$V_2O_5\ (l) + NiO\ (l) \rightarrow NiV_2O_6\ (l) \quad (8)$$

$$V_2O_5\ (l) + Cr_2O_3\ (l) \rightarrow 2CrVO_4\ (l) \quad (9)$$

$$V_2O_5\ (l) + Al_2O_3\ (l) \rightarrow 2AlVO_4\ (l) \quad (10)$$

Figure 5 displays the X-ray diffraction patterns of NiCoCrAlY coatings following 4 hours of hot corrosion testing at 900°C using a Na_2SO_4-50%V_2O_5 salt mixture. The diffraction pattern reveals distinct peaks corresponding to spinel phases [(Ni, Co) Al_2O_4 and (Ni, Co) Cr_2O_4] and oxide phases [(Ni, Co) O, Cr_2O_3, and Al_2O_3]. The oxide phases serve as effective barriers against corrosive species penetration (particularly sulfates in sulfur-containing environments), while the spinel phases function as protective barriers due to their excellent thermal stability and chemical resistance. However, this protective mechanism is only effective when the formed layer is continuous, adherent, and stable.

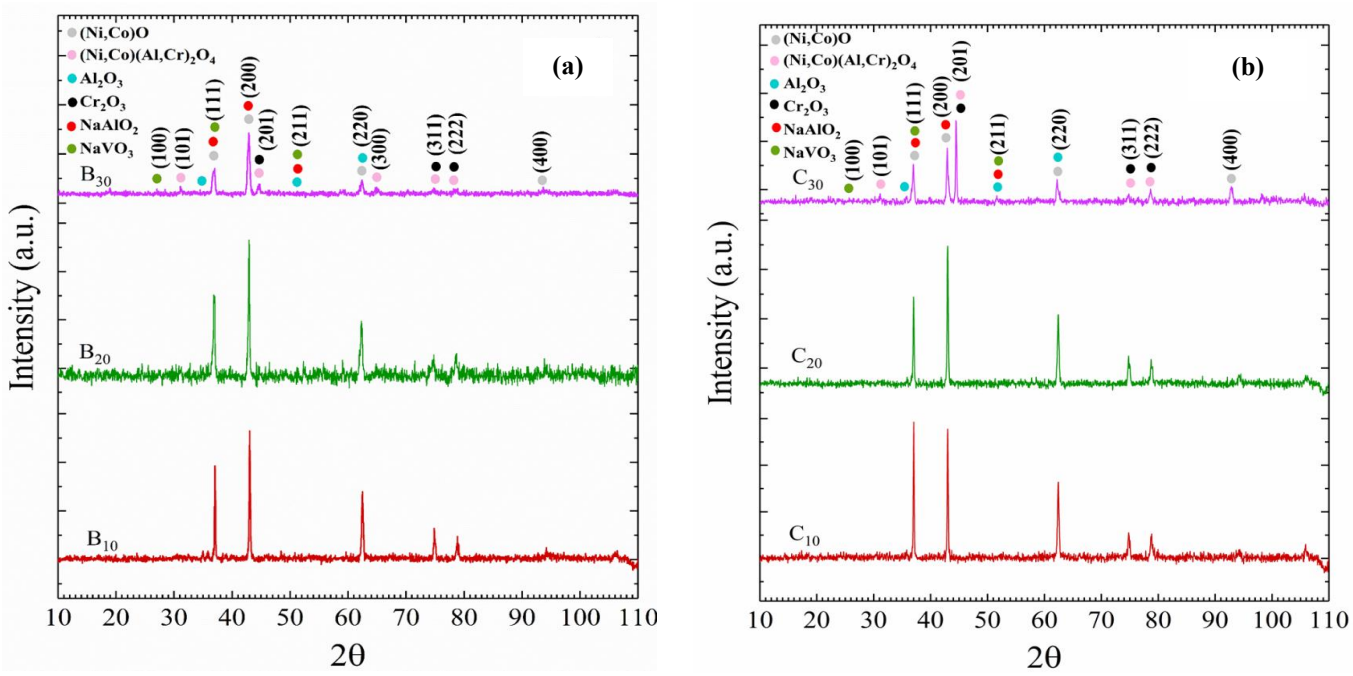

Fig. 5. XRD test results of NiCoCrAlY coatings after 4 h of hot corrosion at 900 °C. a) Current density 20 mA/cm^2 at three powder concentrations 10 – 20 – 30 g/l, b) Current density 30 mA/cm^2 at three powder concentrations 10 – 20 – 30 g/l.

The formation of discontinuous and porous oxides facilitates the penetration of corrosive agents beneath the oxide layer, inhibits the development of a dense alumina scale, and ultimately leads to coating degradation over time. As demonstrated in previous studies (Reaction 7), Al_2O_3 reacts with Na_2SO_4 to form sodium aluminate ($NaAlO_2$), confirming that the hot corrosion process is governed by a basic fluxing mechanism. This mechanism involves: (1) high solubility of the oxide in the molten salt basic flux, and (2) subsequent anion formation. Furthermore, XRD analysis reveals that the coating deposited at 20 mA/cm^2 current density with 20 g/l NiCrAlY powder concentration exhibits significantly higher peak intensities for aluminum oxide phases compared to other specimens. These oxides constitute the primary components of the thermally grown oxide (TGO) layer, as evidenced by their dominant diffraction peaks.

A critical degradation mechanism influencing the material's corrosion rate involves the formation of $NiCr_2O_4$ spinel phase on sample surfaces and chromium/nickel oxides. The $NiCr_2O_4$ spinel forms through the reaction $Cr_2O_3 + NiO \rightarrow NiCr_2O_4$, which subsequently: (1) inhibits oxygen diffusion through the coating, and (2) reduces corrosion rates. Figure. 6a reveals that although sample B_{20} contains a higher quantity of $NiCr_2O_4$ compared to C_{20}, it exhibits superior hot corrosion resistance due to the formation of a continuous spinel layer. The primary mechanism explaining these corrosion differences relates to grain boundary morphology - a fine, compact microstructure can significantly retard corrosion by distributing the same quantity of corrosive salts over a larger surface area at grain boundaries.

Table 4 presents the grain sizes calculated using the Debye-Scherrer method. The results demonstrate that increasing the powder concentration in the deposition bath leads to grain refinement in the coatings. According to the Hall-Petch relationship, this grain refinement enhances the coating's hot corrosion resistance. However, excessive powder concentrations (>30 g/l) promote particle agglomeration and induce Microvoid formation in NiCoCrAlY coatings, consequently degrading their hot corrosion performance. Furthermore, cross-sectional elemental analysis reveals that higher current densities (20 – 30 mA/cm^2) increase powder incorporation into the coatings, which correspondingly improves their hot corrosion resistance through enhanced protective oxide formation.

In our study, samples C_{20} exhibit fewer but deeper and more extensive grain boundaries (Figure. 6b). This observation can be attributed to the distinct grain boundary morphology in C_{20} samples, which contains higher defect densities (e.g., pores) that accelerate corrosion rates. This microstructural feature necessitates post-processing treatments for C_{20} specimens, such as depositing tailored corrosion-resistant layers designed for specific corrosive environments. The penetration of corrosive salts appears inversely correlated with the $NiCr_2O_4$ protective phase content. Nickel chromite ($NiCr_2O_4$) effectively mitigates salt corrosivity by: (1) reducing ionic diffusion pathways, and (2) promoting the formation of additional protective phases. Notably, the coating deposited at 20 mA/cm^2 with 20 g/l NiCrAlY powder concentration demonstrates optimal corrosion resistance, as evidenced by its intact microstructure and minimal salt penetration.

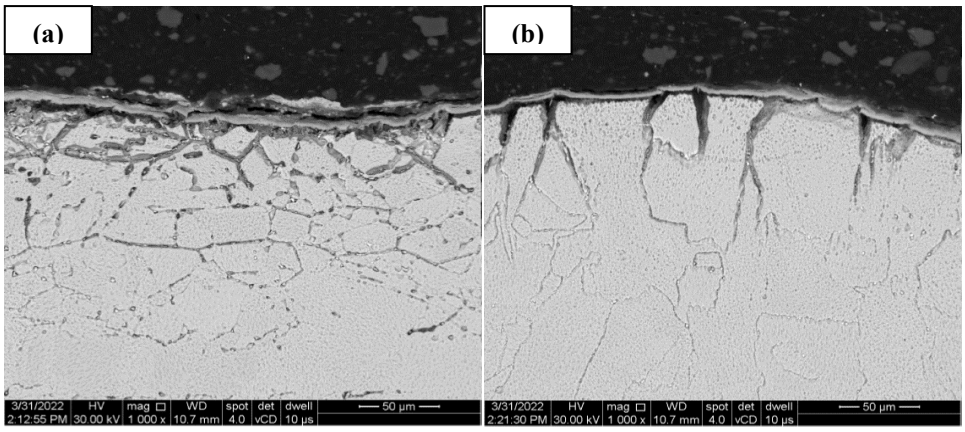

Fig. 6. SEM images with micro-cracks formed at grain boundaries in B_{20} (a) and C_{20} (b) at 900°C/4 h.

Table 4. Grain size values calculated by Debay Scherer method for NiCoCrAlY coatings

Sample	Grain size (Å)	Sample	Grain size (Å)
B_{10}	651.91	C_{10}	768.59
B_{20}	461.92	C_{20}	695.41
B_{30}	623.19	C_{30}	712.73

Figure 7 and 8 present scanning electron micrographs (500× and 1000× magnification) of the NiCoCrAlY coating surface following 4-hour hot corrosion testing at 900°C in the presence of Na_2SO_4-50%V_2O_5 salt mixture. For coatings deposited at 20 mA/cm^2 current density with 10 g/l particle concentration (Figure. 7a), the insufficient chromium and aluminum content (quantified at [X] wt% and [Y] wt%, respectively) prevents the γ' (Al_3Ni) and β (NiAl) phases from forming a continuous, protective alumina scale.

Furthermore, the formation of sodium metavanadate ($NaVO_3$) and its subsequent reaction with alumina significantly accelerates coating degradation. This failure mechanism is similarly observed in coatings prepared at 30 mA/cm^2 current density with 10 g/l particle concentration (Figure. 8a), where the characteristic spallation patterns and porous corrosion products confirm the protective scale's breakdown.

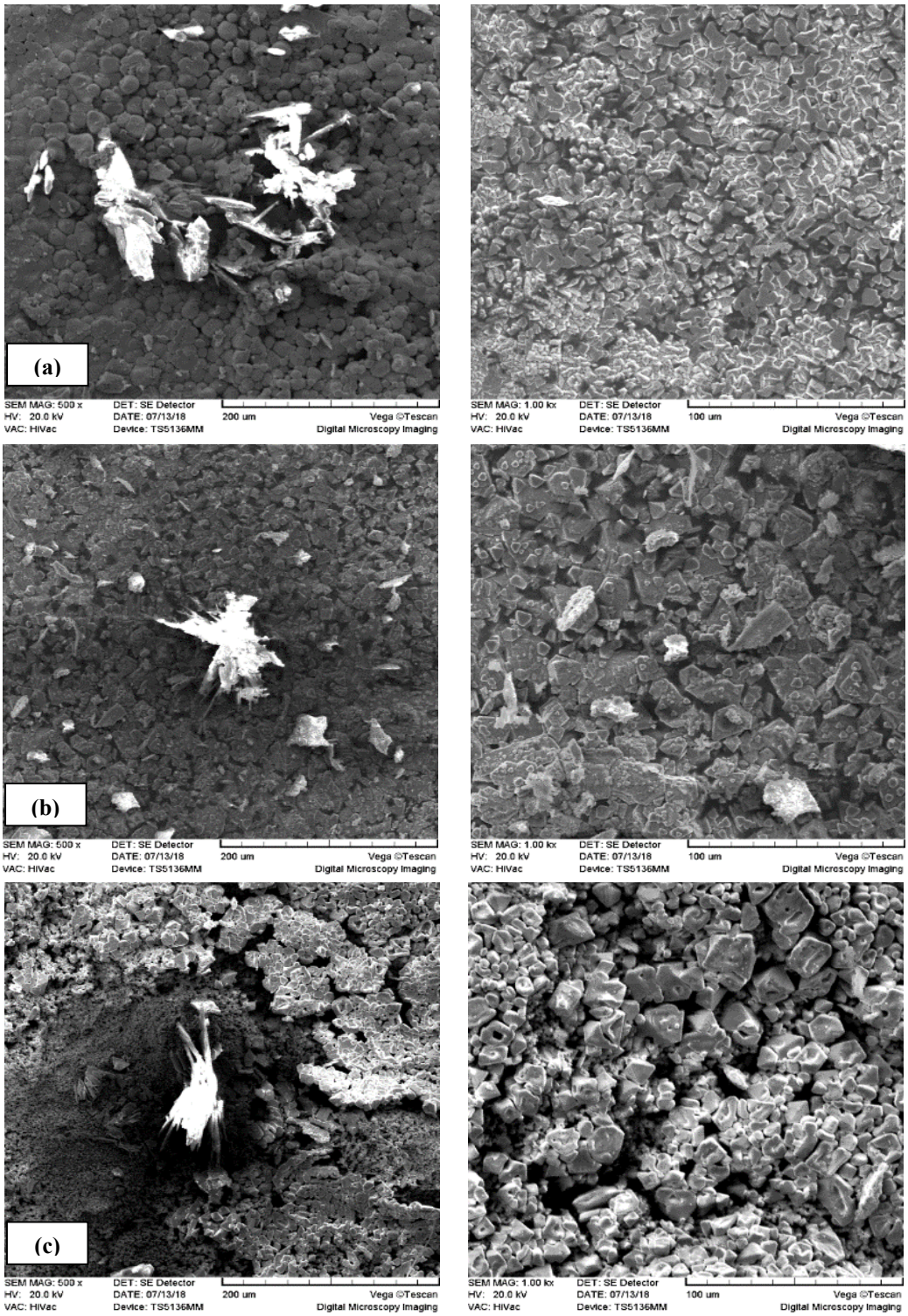

Fig. 7. Surface morphology of NiCoCrAlY coatings after 2 h homogenization treatment at 1100 °C and after 4 h hot corrosion test at 900 °C. a) B_{10}, b) B_{20}, c) B_{30}.

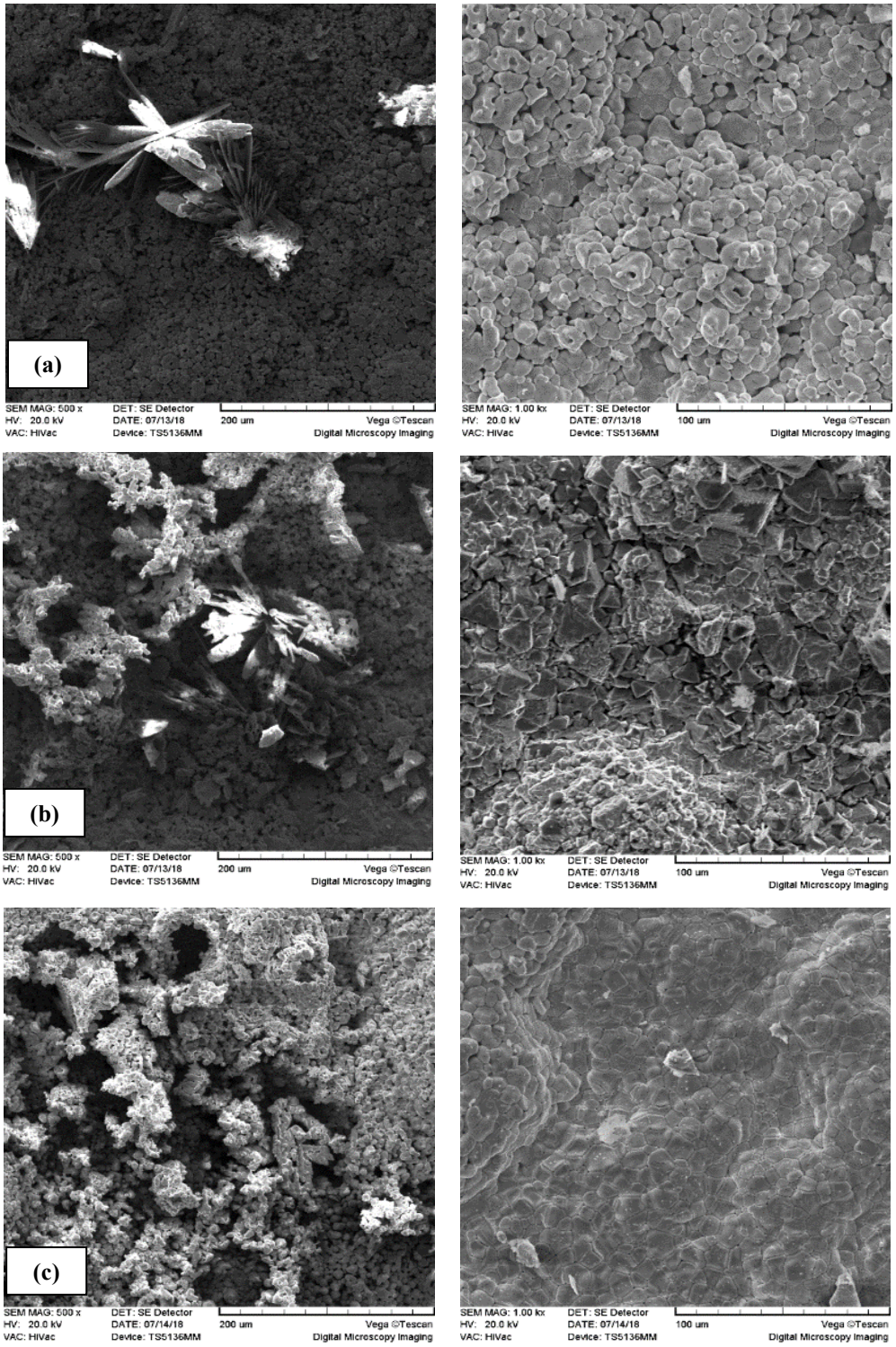

Fig. 8. Surface morphology of NiCoCrAlY coatings after 2 h homogenization treatment at 1100 °C and after 4 h hot corrosion test at 900 °C. a) C_{10}, b) C_{20}, c) C_{30}.

The coating deposited at 20 mA/cm^2 current density with 20 g/l particle concentration (Figure. 7b) demonstrates excellent hot corrosion resistance, maintaining structural integrity without observable cracks or delamination after testing. A similar protective behavior is evident in coatings prepared at 30 mA/cm^2 with 20 g/l concentration (Figure. 8b), though minor microcracking appears on the surface. For coatings fabricated at 20 mA/cm^2 with 30 g/l particle loading (Figure. 7c), while showing superior performance compared to the 10 g/l counterparts, the microstructure reveals: (1) localized pitting corrosion, and (2) deep surface grooves that ultimately compromise coating durability.

This degradation pattern is replicated in specimens prepared at 30 mA/cm^2 with 30 g/l concentration (Figure. 8c), where the combined presence of pits and grooves leads to progressive coating failure.

4. Conclusion

This study provides a comprehensive investigation into the hot corrosion resistance of NiCoCrAlY coatings electrodeposited on Inconel 718LC superalloy substrates under extreme conditions (900°C in Na_2SO_4-50%V_2O_5 molten salt environment). The systematic variation of deposition parameters, including current density (20 and 30 mA/cm^2) and NiCrAlY powder concentration (10, 20, and 30 g/l), revealed critical insights into the coating microstructure-corrosion performance relationship. The optimal coating composition (20 g/l powder concentration at 20 mA/cm^2 current density) demonstrated exceptional resistance to hot corrosion, attributed to the formation of a continuous, adherent layer of protective Al_2O_3 and Cr_2O_3 oxides along with thermally stable (Ni, Co) Cr_2O_4 spinel phases. These phases effectively inhibited the penetration of corrosive species, highlighting the importance of balanced Al and Cr content in the coating matrix.

The degradation mechanisms were elucidated through detailed microstructural and phase analyses, revealing a complex interplay between basic fluxing (Na_2O-induced Al_2O_3 dissolution) and acidic fluxing (V_2O_5-induced oxide scale degradation). Notably, coatings with insufficient Al content (10 g/l) failed catastrophically due to their inability to form a protective alumina scale, while higher powder concentrations (30 g/l) led to particle agglomeration and Microvoid formation, compromising coating integrity. The study also established that grain refinement, achieved through controlled deposition parameters, significantly enhanced corrosion resistance by reducing ionic diffusion pathways along grain boundaries. These findings have important implications for the design of next-generation protective coatings for gas turbine components operating in sulfur-rich environments. The demonstrated correlation between electrochemical deposition parameters and coating performance provides a practical framework for industrial applications. Future research should focus on: (1) optimizing post-deposition heat treatments to further enhance coating homogeneity, (2) investigating the effects of reactive element additions (e.g., Y, Hf) on oxide scale adhesion, and (3) evaluating long-term cyclic corrosion behavior under thermal gradient conditions. This work advances the fundamental understanding of molten salt-induced degradation mechanisms while providing actionable strategies for improving the durability of high-temperature coatings in energy conversion systems.

References

[1] G. Moskal, D. Niemiec, B. Chmiela, P. Kałamarz, T. Durejko, M. Ziętala, T. Czujko, Microstructural characterization of laser-cladded NiCrAlY coatings on Inconel 625 Ni-based superalloy and 316L stainless steel. *Surf. Coat. Technol.*, 387 (2020), 125317. https://doi.org/10.1016/j.surfcoat.2019.12531.

[2] X. Song, J. Lei, J. Xie, Y. Fang, Microstructure and electrochemical corrosion properties of nickel-plated carbon nanotubes composite Inconel718 alloy coatings by laser melting deposition. *Opt. Laser Technol.*, 119 (2019), 105593. https://doi.org/10.1016/j.optlastec.2019.105593.

[3] J. Wang, D. Li, T. Shao, Hot corrosion and electrochemical behavior of NiCrAlY, NiCoCrAlY and NiCoCrAlYTa coatings in molten NaCl-Na2SO4 at 800° C. *Surf. Coat. Technol.*, 440 (2022), 128503. https://doi.org/10.1016/j.surfcoat.2022.128503.

[4] K. Huang, W. Li, K. Pan, X. Lin, A. Wang, Microstructure and corrosion properties of La2Zr2O7/NiCoAlY thermal barrier coatings deposited on Inconel 718 superalloy by laser cladding. *Coatings*, 11, 1 (2021), 101. https://doi.org/10.3390/coatings11010101.

[5] Y. Li, Y. Yang, J. Nie, P. Bai, Z. Liang, S. Wei, … & Q. Guan, Hot corrosion behavior of a NiCoCrAlY coating fabricated by laser cladding on 17-4PH stainless steel. *Eng. Fail. Anal.*, 133 (2022), 105962. https://doi.org/10.1016/j.engfailanal.2021.105962.

[6] T.A. Badea, D. Batalu, N. Constantin, A. Paraschiv, D. Pătroi, L.C. Ceatra, Assessment of hot corrosion in molten Na2SO4 and V2O5 of inconel 625 fabricated by selective laser melting versus conventional technology. *Materials*, 15, 12 (2022), 4082. https://doi.org/10.3390/ma15124082.

[7] L. Li, L. Li, G. Zhang, H. Xue, M. Cui, W. Wang, D. Liu, Hot corrosion behavior of inconel 625 in Na2SO4 and V2O5 molten salt system. *Metals*, 13, 6 (2023), 1069. https://doi.org/10.3390/met13061069.

[8] O. Odabas, Y. Ozgurluk, A.C. Karaoglanli, Hot corrosion behavior of AlCoCrFeNiZr high entropy alloy (HEA) coating system exposed to Na2SO4-V2O5 salt. *Mater. Today Commun.*, 45 (2025), 112289. https://doi.org/10.1016/j.mtcomm.2025.112289.

[9] P. Zamani, Z. Valefi, Hot corrosion resistance of Al2O3 nanoparticles reinforced CoNiCrAlY coatings deposited by LPPS and HVOF processes in molten Na2SO4-V2O5 at 850° C. *Surf. Coat. Technol.*, 472 (2023), 129949. https://doi.org/10.1016/j.surfcoat.2023.129949.

[10] (a) R. Sobhanverdi, A.R. Akbari, Porosity and microstructural features of plasma sprayed Yttria stabilized Zirconia thermal barrier coatings. *Ceram. Int.*, 41 (2015) 14517–14528. https://doi.org/10.1016/j.ceramint.2015.07.102; (b) H. Zhen, X. Peng, A new approach to manufacture oxidation-resistant NiCrAl overlay coatings by electrodeposition. *Corros. Sci.*, 150 (2019) 121-126. https://doi.org/10.1016/j.corsci.2019.01.039; (c) J. Wanga, H. Jia, M. Chena, Z. Bao, S. Zhu, F. Wang, High temperature oxidation and interdiffusion behavior of recoated NiCoCrAlY coating on a nickel-based superalloy. *Corros. Sci.*, 175 (2020), 108894. https://doi.org/10.1016/j.corsci.2020.108894.

[11] B.L. Bates, L.Z. Zhang, Y. Zhang, Electrodeposition of Ni matrix composite coatings with embedded CrAlY particles. *Surf. Eng.*, 31, 3 (2015), 202-208. https://doi.org/10.1179/1743294414Y.0000000376.

[12] B.L. Bates, J.C. Witman, Y. Zhang, Electrolytic co-deposition of Ni-CrAlY composite coatings using different deposition configurations. *Mater. Manuf. Process.*, 31, 9 (2016), 1232-1237. https://doi.org/10.1080/10426914.2015.1090596.

[13] M. Bahamirian, S.K. ASL, An Investigation on effect of bond coat replacement on hot corrosion properties of thermal barrier coatings. *Iran. J. Mater. Sci. Eng.*, 10 (2013), 12-21. http://ijmse.iust.ac.ir/article-1-571-en.html.

[14] I. Keller, D. Naumenko, W.J. Quadakkers, R. Vaßen, L. Singheiser, Influence of vacuum heat treatment parameters on the surface composition of MCrAlY coatings. *Surf. Coat. Technol.*, 215 (2013) 24–29. https://doi.org/10.1016/j.surfcoat.2012.09.066.

[15] (a) X. Peng, S. Jiang, J. Gong, X. Sun, C. Sun. Preparation and Hot Corrosion Behavior of a NiCrAlY + AlNiY Composite Coating. *J. Mater. Sci. Technol.*, 32, 6 (2016) 587–592. https://doi.org/10.1016/j.jmst.2016.04.017; (b) L.Z. Zhang, B.L. Bates, Y. Zhang, Effect of post-deposition heat treatment on electrodeposited NiCoCrAlY coatings. *Mater. Sci. Technol.*, 32, 11 (2016) 1156-1162. https://doi.org/10.1080/02670836.2015.1133022.

[16] (a) T. T. Uzah, I. J. Mbonu, Insight into synergistic corrosion inhibition of thiourea and ZnCl2 on mild steel: Experimental and theoretical Approaches. *J. Chem. Lett.*, 4(4) (2024) 211–221. https://doi.org/10.22034/jchemlett.2024.413932.1135; (b) M. Sheydaei, M. Edraki, Anticorrosion, thermal, and mechanical evaluation of epoxy coatings containing Garcinia cambogia-modified clay, *Chem. Res. Technol.*, 1(3) (2024) 108–113. https://doi.org/10.22034/chemrestec.2024.463954.1020; (c) M. Edraki, M. Sheydaei, D. Zaarei, A brief review of the performance of azole-type organic corrosion inhibitors. *Chem. Rev. Lett.*, 6(1) (2023) 79–85. https://doi.org/10.22034/crl.2023.392268.1221; (d) M. Edraki, D. Zaarei, I. S. Hasan, The impact of green corrosion inhibitors on the protection performance of hybrid silane sol–gel coatings: A review. *Chem. Rev. Lett.*, 6(4) (2023) 428–441. https://doi.org/10.22034/crl.2023.425019.1259.

[17] (a) F. Iorhuna, A. S. Muhammad, A. M. Ayuba, A. T. Nyijime, Molecular dynamic simulations and quantum chemical studies of nitrogen based heterocyclic compounds as corrosion inhibitors on mild steel surface. *Chem. Rev. Lett.*, 6(2) (2023) 114–127. https://doi.org/10.22034/crl.2023.400989.1226; (b) M. G. Udoisoh, E. O. Ajoku, A. G. Sherif, N. N. Chimezie, F. O. Ifeanyi-Nze, I. E. Akemu, G. A. Akpowu, E. M. Adache, M. F. Ajayi, A. E. Omolusi, R. A. Awe, O. O. Omoseyindemi, F. A. Zoum, O. M. Afiari, C. J. Ozoude, S. U. Aiso, K. I. Abdullahi, A. O. Odukoya, I. J. Ojo, Corrosion inhibition of mild steel by ethanol extract of Vernonia amygdalina: Effects of inhibitor concentration and time. *Prog. Chem. Biochem. Res.*, 7(3) (2024) 225–238; (c) V. O. Emelu, C. Emelu, B. B. Babatunde, E. Wali, O. O. Afolabi, Associated Disaster Risk of Inadequate Corrosion Control (Cathodic Protection) on Pipelines in Port Harcourt, Nigeria: A Quantitative Approach. *J. Eng. Ind. Res.*, 4(1) (2023) 22–30; (d) S. R. Tunio, S. Munir, M. Ayaz, F. Ahmad, An Overview of Corrosion Types, Corrosion Testing and Strategies to Inhibit Corrosion. *J. Eng. Ind. Res.*, 5(4) (2024) 204–227.

[18] (a) T. T. Uzah, DFT and Monte Carlo simulation for the prediction of corrosion inhibitive efficacy of selected thiosemicarbazide derivatives on Al (111) and Cu (111) surfaces in acidic media. *J. Med. Nanomater. Chem.*, 6(1) (2024) 81–94; (b) U. I. Shehu, B. Usman, Electrochemical and thermodynamic investigation of Tapinanthus globiferus leave extract as corrosion inhibitor in 0.5 M HCl. *Adv. J. Chem. Sect. B: Nat. Prod. Med. Chem.*, 7(2) (2025) 109–119; (c) A. M. Sanusi, B. B. Roba, B. Usman, Corrosion inhibition by Piliostigma thoningii extract on mild steel in acidic environment: RSM and molecular modeling approach. *Prog. Chem. Biochem. Res.*, 7(1) (2024) 79–99; (d) M. Sajjadnejad, V. T. Targhi, S. M. S. Haghshenas, Evaluation of hot corrosion of hot dip aluminized coated superalloy IN738LC in melted Na_2SO_4–25wt% NaCl salt. *Prog. Chem. Biochem. Res.*, 7(2) (2024) 182–197.

[19] V. Razmgir, NiCrAlY coatings on Inconel718LC super alloy via electrodeposition followed by post deposition annealing. *Chem. Rev. Lett.* 8, 4 (2025) 813-828. https://doi.org/10.22034/crl.2025.515781.1574.

[20] M.S. Mehr, A.R. Akbari, E. Damerchi, Electrodeposited Ni-B/SiC micro- and nano-composite coatings: A comparative study. *J. Alloys Compd.*, 782 (2019), 477-487. https://doi.org/10.1016/j.jallcom.2018.12.184.

[21] A.R. Patil, S.T. Vagge, Hot corrosion behaviour of Inconel 738 superalloy in presence of NaCl, Na2SO4, V2O5. *Mater. Today: Proc.*, 65 (2022), 74-80. https://doi.org/10.1016/j.matpr.2022.05.068.

[22] M. Mirzaei Saatlo, H. Jamali, S. Moradi Alavian, E. Asghari, R. Teimuri Mofrad, M.D. Esrafili, 4-Ferrocenylbutyl-based corrosion inhibitors for mild steel in acidic solution. *Mater. Chem. Phys.*, 293 (2023), 126895. https://doi.org/10.1016/j.matchemphys.2022.126895.

[23] D.G. He, Y.C. Lin, Y. Tang, L. Li, J. Chen, M.S. Chen, X.M. Chen, Influences of solution cooling on microstructures, mechanical properties and hot corrosion resistance of a nickel-based superalloy. *Mater. Sci. Eng., A*, 746 (2019), 372-383. https://doi.org/10.1016/j.msea.2019.01.015.

[24] Z. Chen, T. Dong, W. Qu, Y. Ru, H. Zhang, Y. Pei, S. Li, Influence of Cr content on hot corrosion and a special tube sealing test of single crystal nickel base superalloy. *Corros. Sci.*, 156 (2019), 161-170. https://doi.org/10.1016/j.corsci.2019.05.001.

[25] W. Qu, Z. Chen, Z. Zhang, X. Li, F. Yang, J. Wang, F. Wang, Characteristics and hot corrosion behavior of NiCrAlY metal bonding layers prepared by different processes. *npj Mater. Degrad.*, 8, 1 (2024), 36. https://doi.org/10.1038/s41529-023-00411-z.

[26] H. Jamali, S. Moradi Alavian, E. Asghari, M.D. Esrafili, E. Payami, R. Teimuri Mofrad, Prolonged corrosion protection via application of 4-ferrocenylbutyl saturated carboxylate ester derivatives with superior inhibition performance for mild steel. *Sci. Rep.*, 14, 1 (2024), 13847. https://doi.org/10.1038/s41598-024-64471-0.